

The source of the midwinter suppression in storminess over the

North Pacific

SANDRA PENNY

**Department of Atmospheric Sciences, University of Washington, Seattle, WA*

GERARD H. ROE

Department of Earth and Space Sciences, University of Washington, Seattle, WA

DAVID S. BATTISTI

Department of Atmospheric Sciences, University of Washington, Seattle, WA

** Corresponding author address:* Sandra Penny, Dept. of Atmos. Sci, University of Washington,
408 ATG Bldg., Box 351640, Seattle, Wa 98195-1640
E-mail: smpenny@atmos.washington.edu

ABSTRACT

Feature tracking techniques are employed to investigate why there is a relative minimum in storminess during winter within the Pacific storm track (the midwinter suppression). It is found that the frequency and amplitude of disturbances entering the Pacific storm track from mid-latitude Asia is substantially reduced during winter relative to fall and spring, and the magnitude of this reduction is more than sufficient to explain why there is a wintertime minimum in wave activity over the Pacific. Growth rates of individual disturbances are calculated and compared to expectations from linear theory for several regions of interest. While there are significant discrepancies between linear expectations and actual growth rates over the Pacific, the growth of disturbances within the Pacific storm track cannot explain why the midwinter suppression exists. Furthermore, it is determined that the development of a midwinter suppression over mid-latitude Asia is entirely consistent with linear expectations, which predict a wintertime minimum in Eady growth rates in this region, mainly due to increased stability. Several other mechanisms that may contribute to the development of the midwinter suppression over mid-latitude Asia are discussed, including the interaction between upper-level waves and topography, the behavior of waves upwind of the Tibetan plateau, and the initiation of lee cyclones.

1. Introduction

The midwinter suppression of the Pacific storm track¹ is a striking phenomena for which a complete explanation has proven elusive. In the mid-latitudes, temperature gradients and jet stream winds reach a maximum in the middle of winter. A simple interpretation of the linear Eady model of baroclinic storm formation and growth (Eady 1949; Lindzen and Farrell 1980) predicts that mid-latitude storminess should also maximize at this time, and it does throughout most of the Northern Hemisphere. In the western Pacific, however, many standard Eulerian measures of storminess (e.g., variance of geopotential height) exhibit a relative minimum in winter compared with fall and spring (Fig. 1a).

Nakamura (1992) first identified the midwinter suppression, and since then substantial progress has been made in characterizing it. An intriguing feature of storminess over the Pacific Ocean is that when the strength of the jet stream exceeds $\sim 45ms^{-1}$, the correlation between zonal wind at 250-hPa and many common measures of storminess becomes negative (Nakamura 1992). In addition, a similar relationship exists for inter-annual variability; years with a strong midwinter suppression tend to exhibit stronger-than-normal jet stream winds and vice versa for a weak midwinter suppression (e.g., Chang 2001; Nakamura et al. 2002). In addition, Christoph et al. (1997) concluded that the suppression is not a statistical artifact. That is, it exists in frequencies well outside the range of a typical band-pass filter. Furthermore, the midwinter suppression is a robust feature of the atmospheric circulation that

¹There is some ambiguity in the meaning of the phrase “storm track.” In this study we reserve the phrase “storm track” to refer to the geographic region of enhanced synoptic activity in the climatological sense (as is conventional in climate literature), and not the path of an individual storm. Related to this, we refer to the strength of synoptic activity in a storm track as the amplitude of “storminess.”

is observed in reanalysis data and output from general circulation models (e.g., Nakamura 1992; Zhang and Held 1999; Chang 2001; Yin 2002).

Numerous publications have evaluated how the midwinter suppression may arise through various dynamical mechanisms that occur within the Pacific storm track. A large body of work evaluates the possibility that the faster, narrower, more subtropical wintertime jet stream causes the midwinter suppression. The strong wintertime jet stream, which results in 15% faster group velocity of wave packets within the storm track (Chang 2001), causes propagating waves to be advected quickly through regions of strong baroclinicity and may result in reduced spatial growth rate of storms. However, Nakamura et al. (2002) considered both the increase in group velocity and the increase in expected Eady growth rates, and find that the two together can only explain 5% of the inter-annual variability between Januaries with strong and weak storm activity. Harnik and Chang (2004) explored whether modifications to the linear models accounting for a narrower, faster jet stream can explain the midwinter suppression. They concluded that the process that may be important for inter-annual variability, but the width of the jet stream doesn't vary enough from fall through to spring for it to be of central importance. Deng and Mak (2005) studied a linear β -plane model and find that deformation associated with the strong, narrow wintertime jet stream could be an important factor in the midwinter suppression. However, several other analyses showed that this process may actually work in the *wrong* direction for the seasonal cycle of the Pacific storm track (Chang 2001; Yin 2002; Chang and Zurita-Gotor 2007); transient waves in the Pacific storm track should lose *less* energy to the background flow in winter than fall or spring. Finally, Nakamura and Sampe (2002) showed that the equatorward displacement of the wintertime jet stream causes disturbances to become trapped within a strong subtropical

waveguide during winter. They point out that the more subtropical and consequently less eddy-driven nature of the wintertime jet stream may be centrally important to understanding the midwinter suppression.

Several studies have evaluated the role of diabatic effects in modulating the seasonal cycle of storm activity over the Pacific Ocean. Results, which are drawn from a variety of analysis methods, a broad range of data sources, and a comprehensive hierarchy of models, clearly show that dry dynamics alone cannot fully explain the seasonal cycle of mid-latitude storm activity (Zhang and Held 1999; Chang 2001; Yin 2002; Chang and Song 2006; Chang and Zurita-Gotor 2007). However, the extent to which moist dynamics are responsible for the midwinter suppression is still a subject of debate.

Finally, it is possible that the midwinter suppression is the direct consequence of wave activity *upstream* of the Pacific storm track. Nakamura (1992) and others have noted that a wintertime minimum in Eulerian variance extends well into Asia. Robinson and Black (2006) found evidence that the central magnitude of cyclonic perturbations entering the Pacific storm track during winter is reduced relative to fall and spring. In addition, Robinson et al. (2006) demonstrated that specific patterns in the wintertime mean circulation over Siberia, perhaps associated with modulations of the East Asian winter monsoon, can precede intense wave activity downstream in the Pacific storm track. In a study focusing on the synoptic development of individual troughs, Myoung and Nielsen-Gammon (2009, in preparation) found that deformation may play a role in suppressing the intensity of disturbances upstream of the Pacific storm track.

The work mentioned above comprises a significant contribution to our current understanding of the dynamics that control mid-latitude storminess. When taken together, the

literature suggests that there is no dominant underlying source of the midwinter suppression. Rather, the suppression is the result of several effects that add together to produce a wintertime minimum in synoptic-scale variance.

We demonstrate in this study that a very clear picture of the midwinter suppression emerges when feature tracking is employed to characterize the western Pacific storm track. We show that storminess is reduced in the middle of the winter because the number and amplitude of seed disturbances entering the Pacific is reduced compared to the shoulder seasons. We find no evidence that the structure or growth rate of individual features within the Pacific storm track gives rise to the midwinter suppression. Rather, we show that reduced number of seeds formed well upstream of the Pacific - likely due to the seasonality in the interaction between surface stability, the orography, and upper-level waves over Asia - is the predominant source of the midwinter suppression of storminess in the western North Pacific.

2. Methods

Storm tracks are usually defined as bands of higher than normal synoptic-scale baroclinic wave activity. In the climate literature they are predominantly represented by Eulerian eddy statistics, usually calculated as the variance in a field (such as sea level pressure or heat transport) that has been band-pass filtered to isolate wave activity on the time scale of synoptic storms (e.g., Blackmon 1976; Blackmon et al. 1977). However, with the recent introduction of accurate feature tracking algorithms, it is now possible to objectively calculate storm tracks from the individual disturbances that comprise them.

We have used the feature-tracking algorithm written by Kevin Hodges (Hodges 1994,

1995, 1999) to compile an inventory of all Northern Hemisphere disturbances in the 6-hourly ERA-40 reanalysis dataset (Uppala et al. 2005) from 1958-2001. The algorithm is well documented in the above references, and so we give only a brief description here². The tracking algorithm first identifies all extrema above and below a user-specified minimum threshold value in each time frame for the chosen field. Individual feature paths are then compiled using two constraints, which are chosen adaptively for each disturbance: smoothness of track and appropriate velocity. Finally, all disturbances that do not travel at least 1000-km and last 2 days are thrown out as being too short-lived to be of interest.

In the results section below, we primarily analyze tracking results derived from upper-level (300-hPa) geopotential height for cyclonic disturbances. Results from relative vorticity are also discussed in Appendix A. Synoptic disturbances in these two fields are ideal to track because, after filtering out a background state, features have an easily identified center and central magnitude is a meaningful measure of intensity. The minimum threshold value (relative to the background field) for the existence of a feature is chosen as $3 - dm$ for geopotential height and 10^{-5} s^{-1} for relative vorticity (Appendix A). We find that the algorithm is insensitive to any reasonable choice of minimum threshold and the that lifetime and track length requirements ensure that only substantial disturbances are included in the analysis.

In identifying features to track, it is often necessary to subtract a background field so that only synoptic features are retained, and this is often done by first processing the data through a temporal or spatial filter that admits only synoptic-scale disturbances. For geopotential height, we subtract the seasonal cycle through application of a 90-day high-pass Butterworth

²On Kevin Hodges' website, seasonal climatologies of feature tracking results from the ERA-40 dataset available for download. View www.nerc-essc.ac.uk/kih/AMIP2/era40_results.html for more details.

filter and then we apply a spatial filter that admits only planetary wave numbers between 5 and 42. As this is a slightly unconventional filtering method, some discussion is warranted.

For our purposes, a standard temporal filter such as a 2.5-6 day band-pass filter (e.g., Blackmon 1976; Blackmon et al. 1977) is not ideal because it over-emphasizes the wave-like nature of the atmosphere and artificially adds disturbances where none existed in the original field. This is only a small disadvantage for Eulerian storm tracks, where storminess is often measured by the standard deviation of a field, but this is an undesired effect when using feature tracking.

To avoid complications associated with temporal filters, Hoskins and Hodges (2002, 2005) and Anderson et al. (2003) advocate for the use of a planetary spatial filter. However, Donohoe and Battisti (2009, accepted and revised) recently showed that the planetary filter retains significant amplitude time-average features in the core of the Pacific and Atlantic storm tracks (of the order 10-hPa or more for the field of sea-level pressure). Consistent with their results, we find that not only is the magnitude of individual geopotential height disturbances impacted by these artificial time-mean features, the number of disturbances identified by the tracking algorithm is also affected (not shown). This is a considerable drawback to the planetary spatial filter.

We find that combining a planetary spatial filter with a seasonal mean filter does much to avoid all of the above limitations. The seasonal mean filter decreases the amplitude of time-averaged spatial features by almost two orders of magnitude, from around 10-hPa to ~ 0.3 -hPa without affecting synoptic motions. This effectively eliminates the largest drawback associated with a planetary spatial filter and retains its advantages over a band-pass filter.

In order to distinguish between different geographic areas, we define the western Pacific

storm track as being comprised of disturbances that cross the longitude 160°E , between 20° - 70°N . This choice is made to focus on the region that, in eddy statistics, has a strong midwinter suppression (see Fig. 1). For illustration, Figure 2 shows a sample of the paths of cyclonic disturbances (randomly selected from the month of November) tracked in geopotential height at 300-hPa.

The analysis is not sensitive to this choice of location; similar results are obtained when performing the same analysis throughout the western and central Pacific. Results are also insensitive to the latitudinal range, for example results are essentially the same if tracking all disturbances between 20° - 70°N or only those located within 10 degrees to the north and south of the climatological storm track axis. Results found using the whole record (1958-2001) also hold for the satellite era (1979-2001). Though most of the results we present here are found in the field of geopotential height, we have performed similar calculations using vorticity, meridional wind and zonal wind at levels between 250-hPa and 1000-hPa. Tracking results from these fields (not shown) are very similar, and there are some interesting considerations for tracking relativorticity that are explained in Appendix A.

3. The midwinter suppression characterized by the number and amplitude of disturbances

a. Tracking results for upper-level geopotential height

The midwinter suppression of the Pacific storm track was first identified by Nakamura (1992), and his calculation (updated to include data from the ERA-40 dataset, 1958-2001)

is reproduced in Fig. 1. Over the North Atlantic Ocean, upper-level geopotential height variance is maximized in the middle of winter, whereas over the western North Pacific it peaks during fall and spring. Along the longitude band 160°E between $20\text{-}70^{\circ}\text{N}$ (marked as the bold line in Figure 2), the variance of geopotential height at 300-hPa is reduced by approximately 25% in winter relative to the shoulder seasons.

Feature tracking enables changes in storminess to be studied in greater detail. In particular it is possible to isolate the relative importance of changes in feature frequency and changes in feature strength, which is impossible using Eulerian eddy statistics alone. In Appendix B we discuss the link between Eulerian variance and the results obtained by feature tracking. We obtain climatological data on the frequency of occurrence and the average central magnitude of all disturbances that cross 160°E and 50°W for the Pacific and Atlantic storm tracks, respectively, for each calendar day; these results are shown in Fig. 3. A 31-day running mean smoother is applied before plotting the results to reduce noise and represent the data in terms of monthly averages. Over the Atlantic Ocean feature strength is maximized during winter, and feature number exhibits little seasonality. In contrast, the disturbances within the Pacific storm track show a clear reduction in both number ($\sim 20\%$) and amplitude ($\sim 14\%$) during winter compared to spring and fall. These results are robust well above the 95% confidence level determined from a student's t-test, and is observed in all locations throughout the western North Pacific domain, from 120°E to 160°W .

Nakamura (1992) speculated that a wintertime lull in the generation of seed disturbances over Asia could play a role in the suppression of storminess in the western Pacific. We investigate this possibility by separately considering the Pacific disturbances that have their genesis over land and those that originate over water, shown in Fig. 4. The frequency of

cyclones over the Pacific Ocean steadily increases from October (~ 3 per month) through to April (~ 5 per month) and the amplitude of these disturbances is relatively constant throughout the cold season. On the other hand, cyclogenesis over land is significantly reduced in midwinter relative to fall and spring, by about 40% in frequency and 20% in amplitude. This is a strong indication that a reduction in the frequency of seeds from Asia is responsible for the midwinter suppression.

The presence of the Tibetan plateau causes the storm track over Asia to split into two branches: a mid-latitude branch to the north and a subtropical branch to the south. It is widely accepted that the storm track over the Pacific Ocean is primarily seeded by waves propagating from the mid-latitude branch over northeast Asia (e.g., Wallace et al. 1988; Hakim 2003), but recent work shows that wave activity within the Pacific storm track can be seeded by both branches (Hoskins and Hodges 2002; Chang 2005). We also find that disturbances that exist over the western and central Pacific Ocean can have both mid-latitude and subtropical origins. We investigate the relative importance of the northern and the southern branch (Fig. 5), and then we consider the impact of influences upwind of Tibet (Fig. 6).

The features that cross the longitude 160°E between 20°N - 70°N are separated by their latitude of cyclogenesis³, using 40°N as the dividing line, in Fig. 5. Consistent with previous studies, the mid-latitude branch comprises the majority of the disturbances downstream in the Pacific storm track. Both the frequency and amplitude of disturbances that originated to the north of 40°N show a clear wintertime reduction. In contrast, the number of features that originate south of 40°N steadily increases from fall through to spring and the amplitude of

³We define cyclogenesis location as the location that the tracking algorithm first identifies a feature.

these features is largest during the winter months. This strongly suggests that the midwinter suppression is not caused by changes in subtropical cyclogenesis and/or subtropical seeding.

Next, we calculate the frequency and amplitude of features upwind of the Tibetan plateau, as they cross 60°E (Fig. 6 a, b), and downwind, as they cross 120°E (Fig. 6 c, d). Upwind of the plateau, there is a wintertime maximum in the number of disturbances and a maximum in their amplitude during fall. This is in contrast to the situation directly downwind of the Tibetan plateau, where the midwinter suppression is clearly seen as the reduction of both the frequency and amplitude. From the above discussion and results, we find that the midwinter suppression in storminess over the North Pacific Ocean has its origins over mid-latitude Asia, to the north of the Tibetan plateau.

4. The role of changes in growth rates for the midwinter suppression

We have shown that the midwinter suppression can be understood by considering the behavior of upper-level waves *upwind* of the Pacific storm track. Therefore, there is no need to invoke changes in the development of disturbances within the storm track itself as an explanation for the midwinter suppression. Nonetheless, several studies have found compelling evidence that the structure and growth rates of barclinic waves within the Pacific storm track may be modified due to the seasonal cycle of the background flow in a way that causes the midwinter suppression (e.g., Nakamura 1992; Christoph et al. 1997; Chang 2001; Yin 2002).

To investigate this with our dataset, we calculate the average temporal growth rate of all growing disturbances in several regions, shown in Fig. 7. We measure growth rate in Bergerons ($Bergeron = \frac{Z_2 - Z_1}{6hrs} \frac{\sin(60^\circ)}{\sin(.5(\phi_1 + \phi_2))}$), which is equivalent to the change in central amplitude over one six-hour period, normalized by the Coriolis parameter. We calculate the growth rate of each growing feature that exists within Pacific storm track (20-70°N, 140-180°E), the Atlantic storm track (20-70°N, 30-70°W), and the mid-latitude Asian storm track (40-55°N, 90-120°E) (These regions are shown by the box in Fig. 2). Note that because this growth rate is calculated following the feature, the results in Fig. 7 are independent of changes in the speed of disturbances; that is, the fact that features are traveling faster over the oceans during winter than they are in the shoulder seasons (e.g., Chang 2001) does not affect this calculation.

Observed growth rates and corresponding monthly-averaged near-surface adjusted Eady growth rate (explained below) are co-plotted in Fig. 7a, d, and g. The Eady growth rate is calculated following the methods outlined in Lindzen and Farrell (1980) from the equation

$$\sigma_{MAX} = \frac{f}{N^2} \frac{\partial \bar{u}}{\partial z}. \quad (1)$$

Monthly averages are computed for a “near-surface layer” in a region corresponding to the storm tracks in Fig. 2. This layer corresponds to the layer between 925-hPa and 850-hPa for the Pacific and Atlantic storm tracks, and 850-hPa to 700-hPa for the mid-latitude Asian storm track. A near-surface layer is chosen because Nakamura and Shimpo (2004) found that near-surface Eady growth rates correlate with jet stream-level wave activity better than a layer just above the height of the boundary layer⁴.

Growth rates predicted from the Eady model are traditionally expressed as percent

⁴Our results show that the Eady model is a good diagnostic tool for estimating monthly-averaged growth

growth (as in Eq. 1), whereas our method corresponds to absolute growth. In order to express these two measures with the same units ($dmhr^{-1}$), we devine an “adjusted Eady growth rate” as the product of the Eady growth rate and the average disturbance amplitude from the feature tracking algorithm. For reference, the monthly-averaged feature amplitude of growing disturbances (Fig. 7b, e, and h) and the traditional Eady growth rate (Fig. 7c, f, and i) are also shown. The adjusted and traditional Eady growth rates are intended solely for diagnostic purposes, since the Eady model is only valid for small disturbances in their linear phase of growth whereas we have included all growing disturbances in this calculation.

Within the Atlantic storm track, Fig. 7d, there is a wintertime maximum in the growth rate of individual disturbances and this correspondes well with expectations from linear theory. The same is not true over the Pacific Ocean. While the adjusted Eady growth rate maximizes during winter, actual growth rates are relatively constant through the cold season except for a marked springtime maximum (Fig. 7a). A springtime maximum in actual growth rates is also evident when we consider only the top 1 – 10% of growths, and it is robust to choice of location and calculation method (e.g., for growth rates over 6 to 48 hours, including or excluding negative growths, choice of vertical levels).

Interestingly, there is no evidence of a midwinter minimum in the average growth rate of growing upper-level disturbances over the western and central Pacific (Fig 7a). Therefore, rates. However, it is not a good indicator of growth rates for individual events. For regions within the Pacific and Atlantic storm track, for example, the correlation coefficient between the actual growth rate and the Eady model prediction at the same time and location is found to be between 0.15 and 0.20 (not shown). For this calculation, we have included only small (< 5 or $10dm$) growing disturbances, and the actual correlation varies depending on the region and vertical level. This correlation is statistically significant at well above 99% confidence due to the large number of disturbances included in the analysis.

our observations show that the growth rate of individual disturbances within the Pacific storm track *cannot* explain the existence of the midwinter suppression. Nonetheless, there are clearly large discrepancies between observations and theory, in particular over the Pacific Ocean.

For the mid-latitude Asian storm track there is a marked and statistically significant suppression in both actual and expected Eady growth rates (Fig. 7g). Therefore, our observation that the midwinter suppression in the amplitude of disturbances in the Pacific storm track develops over mid-latitude Asia (Figs. 3a, 4a, 5a, and 6c) is entirely consistent with linear expectations. For example, consider the idealized case of disturbances traveling approximately $12ms^{-1}$ along the latitude $50^{\circ}N$ between $90^{\circ}E$ and $120^{\circ}E$ (a distance of approximately 3700 km). For features initially at $90^{\circ}E$ with identical amplitudes, the observed reduction in wintertime growth rate of $0.03dmhr^{-1}$ would result in a $2.5dm$ reduction in the amplitude of disturbances arriving at $120^{\circ}E$. This compares very well with the actual reduction in amplitude during winter, shown in Fig. 6c. Note that this argument only relates to why a midwinter suppression in feature amplitude develops over mid-latitude Asia. Most individual disturbances do not travel from $90^{\circ}E$ all the way to the Pacific storm track. However, we observe a very similar seasonal cycle in growth rates if we limit our analysis in Fig. 7g to only include features that also make it into the Pacific storm track. Additionally, the wintertime minimum in Eady growth rates suggests conditions are less favorable for cyclogenesis, which helps explain the midwinter suppression in the number of disturbances in this region.

5. Mechanisms that could explain the midwinter suppression

The last section identified the source of the midwinter suppression: the wintertime minimum in the number of disturbances born in Northern Asia and tracking into the Pacific and the wintertime minimum in the growth rate of these disturbances. We now discuss some mechanisms that could cause this reduction in the genesis rate and growth rate of these storms.

The wintertime minimum in Eady growth rates suggests conditions are less favorable for cyclogenesis, which helps explain the midwinter suppression in the number of disturbances in this region. The wintertime reduction in near-surface Eady growth rates is dominated by the seasonality of near-surface static stability (Fig 7h due mainly to the seasonal cycle in local insolation. Change in Eady growth rate due to changes in shear are a secondary effect. Nakamura et al. (2002) demonstrate that inter-annual variability associated with the midwinter suppression is anti-correlated with the strength of a stationary feature, the East Asian winter monsoon. In their paper, they identify East Asian winter monsoonal flow as strongly influenced by the relative strength of the Siberian high-pressure system. These observations all support the possibility that seasonal modulations associated with strong static stability and patterns of high pressure over Asia play a central role in the onset of the midwinter suppression.

A second possible mechanism, also directly related to near-surface effects, concerns the seasonal cycle in lee cyclogenesis. (Hoskins and Hodges 2002) show using feature tracking that most midlatitude lower tropospheric cyclones are born in the lee of mountains. Chen

et al. (1991) showed that there are significantly fewer lee cyclones emanating from the lee of the Altai-Sayan mountains (identified in Fig 2) in winter than fall or spring. In addition, Newton (2004) later noted that there is a striking correlation between the midwinter suppression over the Pacific Ocean and the generation of low-level Altia-Sayan lee cyclones. ? argued that lee cyclogenesis in this region may be suppressed during winter because most of the continent is cold and strong temperature gradients lie well to the south (contributing to the wintertime minimum in Eady growth rates). By contrast, strong surface temperature gradients are frequently observed during fall and spring. We also composited the upper level circulation at the time of lee cyclogenesis. These results (not shown) demonstrate that lee cyclogenesis is usually accompanied by a significant upper-level low that is oriented to the west of its low-level counterpart, an indication that upper- and lower- levels are in a position to mutually reinforce each other. Taken together, these results strongly suggest that lee cyclones play an active role in the development of the midwinter suppression.

Finally, influences upwind of the Tibetan plateau may also be contribute to the winter minimum in the number of disturbances. Hakim (2003) find that a large fraction of wave packets upwind of the Tibetan plateau are diffracted into the subtropical jet stream and decay before entering the Pacific storm track. We have investigated whether waves are preferentially diffracted into the strong subtropical jet core over central Asia in winter. Preliminary results, which will be addressed in the future, show that this may be crucial to the development of the midwinter suppression.

6. Summary

The midwinter suppression in storminess over the western and central Pacific Ocean is due to a reduction in the number of disturbances entering the Pacific storm track from mid-latitude Asia. Feature-tracking reveals that the number and amplitude of disturbances within the storm track in winter is reduced by 15 to 43% and 12 to 24% compared to that of spring and fall, respectively. The exact percentage depends on the variable, level, and geographic location. The reduction in the number and amplitude of disturbances within the Pacific storm track is sufficient to explain the observed midwinter reduction in eddy variances that are documented here and previously (see Appendix B for a comparison between feature tracking and Eulerian variance).

The midwinter reduction in the number and amplitude of storms within the Pacific storm track is not due to local changes in the synoptic scale dynamics associated with seasonal changes in the structure of the jet. For example, there is no mid-winter minimum in the growth rate of synoptic storms within the storm track. Instead, the reduction in the amplitude of storms in the Pacific storm track is due to a midwinter minimum in the growth rate of storms emanating from north Asia, mainly due to the wintertime maximum in static stability.

In addition to the generic stabilization of the atmosphere to baroclinic development by increased static stability, we discuss other mechanisms that might contribute to the midwinter suppression, all of which depend crucially on the interactions between surface stability, the orography and upper-level waves over Asia. Whether one or all of these mechanisms is the cause of the midwinter suppression is the subject of ongoing research.

There are many possible choices for a measure of storminess, and the correct choice is not always obvious. The use of Eulerian statistics has predominated in the study of climatological storminess in part because of its ease of calculation from reanalysis data sets, and in part because such statistics are required in calculating heat and momentum budgets of the atmospheric circulation. However, Eulerian eddy statistics conflate many different aspects of the weather of which that climatology is comprised, and which may be of individual interest: storm number, storm intensity, storm speed, and storm extent all affect the Eulerian statistics. In many regards Lagrangian feature-tracking provides a more fundamental perspective on climate, as it can more directly target the aspects of dynamical weather systems that are felt most keenly by observers on the ground - in other words, high precipitation, high winds, strong frontal passages, etc., during individual storms. The availability of high-quality feature-tracking algorithms therefore continue to provide many new and interesting opportunities for future research.

Acknowledgments.

The authors are very grateful to Kevin Hodges for allowing us to use his feature tracking algorithm, for his assistance with the program's use, and for helpful comments on an earlier version of this paper. Aaron Donohoe contributed to many discussions about this work and about the midwinter suppression in general. This draft was significantly improved by helpful comments and suggestions from Greg Hakim, Justin Minder, and two reviewers. This work was funded by the National Science Foundation Continental Dynamics Grant 6312293.

APPENDIX A

Tracking results for upper-level relative vorticity

Similar results concerning the reduction in the number and amplitude of disturbances during winter are found when tracking upper-level cyclonic relative vorticity⁵ disturbances instead of geopotential height features. It is again clear, from Fig. 8, that the midwinter suppression is primarily a consequence of there being fewer and smaller disturbances in winter than in fall and spring, and that the reductions are due to effects over land (not shown for relative vorticity). However, there are some important and interesting differences in the tracking results for geopotential and relative vorticity at the same pressure level (300-hPa). First, the tracking algorithm identifies almost twice as many disturbances in relative vorticity. This is perhaps not surprising since vorticity features are smaller in spatial scale than are geopotential height features.

Second, it is surprising that the amplitude of relative vorticity features is actually an *absolute minimum* during winter, relative even to summer (Fig. 8a). This is not an artifact of the feature tracking algorithm: the variance of 2-6 day band-pass filtered relative vorticity at 300-hPa is also an absolute minimum in winter at this location (not shown). We should be wary of any measure of storminess if it indicates that the Pacific storm track is more

⁵For tracking features in relative vorticity we take a rather minimalist approach to filtering. The data are first truncated to T42 resolution to reduce noise, and then we subtract out the seasonally-varying background field by applying a 90-day high-pass Butterworth filter. Others find that applying any filter to the field of vorticity is unnecessary for some applications (e.g., Hakim 2003), however without a seasonal mean filter significant amplitude time-average features (of the order $\sim 2 \cdot 10^{-5} s^{-1}$) are retained in the heart of the Pacific storm track, and this is something that we wish to avoid for feature tracking.

intense during summer than it is in the middle of winter.

Scaling arguments having to do with the seasonal cycle of an average feature's areal extent can explain these peculiar results. In the geostrophic limit, relative vorticity is the Laplacian of geopotential height divided by the Coriolis parameter. Consequently, for two features that have the same central magnitude in geopotential height, the one with the largest relative vorticity amplitude is the one that occupies the least area. To determine the seasonal cycle of the average area of disturbances, we use tracking results to identify the center of all features as they cross various longitude bands within the Pacific storm track (i.e., 160°E , 180°) and employ compositing to estimate their average area (not shown). This reveals that the areal extent of disturbances during summer is just over half that of winter. In addition, in October and April features occupy approximately 18% less area than they do in January (not shown), so we cannot ignore this effect for the midwinter suppression. Evidently, we should be wary about interpreting the variance of relative vorticity as a measure of storminess when the areal extent of waves changes significantly.

A notable seasonal cycle to the area of synoptic waves in the atmosphere has been discussed to some extent by Hoskins and Hodges (2005), but to our knowledge this has never been examined in detail. Further, both the meridional and zonal extent of disturbances is maximum in winter, which is surprising because the jet stream is narrower in winter than it is in the shoulder seasons. Ioannou and Lindzen (1986) found that the meridional extent of the jet stream is a reasonable first-order approximation to the meridional wavelength of storms, and based on these results, previous work concerning the midwinter suppression assumed that the meridional wavelength of storms in the Pacific storm track will be less in winter than it is in the shoulder seasons (e.g., Harnik and Chang 2004). The wavelength corresponding

to the most unstable Eady mode depends on the Rossby radius of deformation, and this in turn depends on the ratio of static stability to the Coriolis parameter, both of which may act to increase the Rossby radius. Alternatively, others find evidence that deformation may be responsible for the longer wavelength (Nielsen-Gammon, personal communication). In the future a detailed investigation will undoubtedly reveal interesting insights.

APPENDIX B

Comparing Eulerian variance with feature tracking statistics

Our intention is to understand how the midwinter suppression manifests in terms of the individual disturbances that comprise the Pacific storm track. However, it is worth considering how the results from feature tracking compare to Eulerian variance at the same location.

In order to make such a comparison we start by considering a single sine pulse with period τ traveling by a point (take $x = 0$ for simplicity) in the time interval $[0, T]$, where $\tau \ll T$:

$$Z = Z_0 \sin \frac{2\pi ct}{\lambda}, \quad 0 < t < \tau. \quad (\text{B1})$$

Thus, the variance at this location due to a single traveling pulse is

$$\overline{(Z')^2} = \overline{Z_0^2 \sin^2 \frac{2\pi ct}{\lambda}}, \quad (\text{B2})$$

where c and λ are the velocity and wavelength of the traveling wave, respectively, Z_0 is its amplitude, and $\overline{(\)} = \frac{1}{T} \int_T (\) dt$ is the integral over the time of interest, T . In this

framework, if the number of traveling sine pulses (N) doubles to from one to two, then there is twice as much variance. Therefore the total variance must scale linearly with the number of disturbances passing overhead. Noting that $\int_T \sin^2(at)dt = 1/(2a)$, we see that the Eulerian variance is related to feature tracking in the following way:

$$\overline{(Z')^2} \propto N \cdot Z_0^2 \cdot \lambda \cdot c^{-1} \equiv B_{LAGR}. \quad (\text{B3})$$

Eulerian variance is compared to feature tracking results in Table 1. For these calculations, variance of geopotential height at 300-hPa is the average in the 2-6 day band-pass filtered field along 160°E, between 20-70°N. Data for the number, magnitude, wavelength, and velocity are average values for all disturbances as they cross the same location, 160°E between 20-70°N. In Table 1, fall corresponds roughly to the month of November (Julian days 300-325), winter corresponds to January (days 10-35), and spring corresponds to April (days 90-115). From this information we see that feature tracking statistics predict that the midwinter suppression should manifest as a 39% reduction in the Eulerian variance in winter relative to fall and spring. This is 14% higher than the observed 25% reduction in wintertime variance.

There are several reasons not to expect these calculations to be directly comparable. First, in this paper the focus is on cyclonic disturbances only, yet variance is a combination of both cyclones and anticyclones. Analysis of the number and amplitude of anticyclones at this location (not shown) reveals that high pressure systems do not exhibit a midwinter suppression. Second, Lagrangian statistics include only trackable, mobile disturbances, whereas there is no such requirement for Eulerian techniques. Third, for feature tracking

we have employed both a seasonal mean filter and a planetary wave filter (see discussion in the methods section), however Eulerian variance is traditionally measured as the variance of a band-pass filtered field (for our variance calculations we use a 2-6 day band-pass filter). Finally, and perhaps most importantly, we have greatly simplified the relationship between Eulerian variance and feature tracking by assuming that storm tracks are composed entirely of a series of identical sine pulses. In reality, the amplitude, velocity, and wavelength of disturbances are not necessarily independent of each other nor are they constant from one feature to the next. Given these limitations, the agreement between feature tracking and Eulerian variance is reasonable.

REFERENCES

- Anderson, D., K. I. Hodges, and B. J. Hoskins, 2003: Sensitivity of feature-based analysis methods of storm tracks to the form of background field removal. *Monthly Weather Review*, **131** (3), 565–573.
- Blackmon, M. L., 1976: Climatological spectral study of 500 mb geopotential height of Northern Hemisphere. *Journal of the Atmospheric Sciences*, **33** (8), 1607–1623.
- Blackmon, M. L., J. M. Wallace, N. C. Lau, and S. L. Mullen, 1977: Observational study of Northern Hemisphere wintertime circulation. *Journal of the Atmospheric Sciences*, **34** (7), 1040–1053.
- Chang, E. K. M., 2001: GCM and observational diagnoses of the seasonal and interannual variations of the Pacific storm track during the cool season. *Journal of the Atmospheric Sciences*, **58** (13), 1784–1800.
- Chang, E. K. M., 2005: The impact of wave packets propagating across Asia on Pacific cyclone development. *Monthly Weather Review*, **133** (7), 1998–2015.
- Chang, E. K. M. and S. W. Song, 2006: The seasonal cycles in the distribution of precipitation around cyclones in the western North Pacific and Atlantic. *Journal of the Atmospheric Sciences*, **63** (3), 815–839.
- Chang, E. K. M. and P. Zurita-Gotor, 2007: Simulating the seasonal cycle of the Northern

- hemisphere storm tracks using idealized nonlinear storm-track models. *Journal of the Atmospheric Sciences*, **64** (7), 2309–2331, Chang, Edmund K. M. Zurita-Gotor, Pablo.
- Chen, S. J., Y. H. Kuo, P. Z. Zhang, and Q. F. Bai, 1991: Synoptic climatology of cyclogenesis over East Asia, 1958-1987. *Monthly Weather Review*, **119** (6), 1407–1418.
- Christoph, M., U. Ulbrich, and P. Speth, 1997: Midwinter suppression of Northern Hemisphere storm track activity in the real atmosphere and in GCM experiments. *Journal of the Atmospheric Sciences*, **54** (12), 1589–1599.
- Deng, Y. and M. Mak, 2005: An idealized model study relevant to the dynamics of the midwinter minimum of the Pacific storm track. *Journal of the Atmospheric Sciences*, **62** (4), 1209–1225.
- Donohoe, A. and D. S. Battisti, 2009, accepted and revised: The true asymmetry between synoptic cyclone and anticyclone amplitudes: Implications for filtering methods in Lagrangian feature tracking. *Journal of the Atmospheric Sciences*.
- Eady, E. T., 1949: Long waves and cyclone waves. *Tellus*, **1**, 33–42.
- Hakim, G., 2003: Developing wave packets in the North Pacific storm track. *Monthly Weather Review*, **131** (11), 2824–2837.
- Harnik, N. and E. K. M. Chang, 2004: The effects of variations in jet width on the growth of baroclinic waves: Implications for midwinter Pacific storm track variability. *Journal of the Atmospheric Sciences*, **61** (1), 23–40, 41 AMER METEOROLOGICAL SOC 760NH.

- Hodges, K. I., 1994: A general-method for tracking analysis and its application to meteorological data. *Monthly Weather Review*, **122** (11), 2573–2586.
- Hodges, K. I., 1995: Feature tracking on the unit-sphere. *Monthly Weather Review*, **123** (12), 3458–3465.
- Hodges, K. I., 1999: Adaptive constraints for feature tracking. *Monthly Weather Review*, **127** (6), 1362–1373.
- Hoskins, B. J. and K. I. Hodges, 2002: New perspectives on the Northern Hemisphere winter storm tracks. *Journal of the Atmospheric Sciences*, **59** (6), 1041–1061.
- Hoskins, B. J. and K. I. Hodges, 2005: A new perspective on Southern Hemisphere storm tracks. *Journal of Climate*, **18** (20), 4108–4129.
- Lindzen, R. S. and B. Farrell, 1980: A simple approximate result for the maximum growth-rate of baroclinic instabilities. *Journal of the Atmospheric Sciences*, **37** (7), 1648–1654.
- Nakamura, H., 1992: Midwinter suppression of baroclinic wave activity in the Pacific. *Journal of the Atmospheric Sciences*, **49** (17), 1629–1642.
- Nakamura, H., T. Izumi, and T. Sampe, 2002: Interannual and decadal modulations recently observed in the Pacific storm track activity and east Asian winter monsoon. *Journal of Climate*, **15** (14), 1855–1874.
- Nakamura, H. and T. Sampe, 2002: Trapping of synoptic-scale disturbances into the North-Pacific subtropical jet core in midwinter. *Geophysical Research Letters*, **29** (16).

- Nakamura, H. and A. Shimpo, 2004: Seasonal variations in the Southern Hemisphere storm tracks and jet streams as revealed in a reanalysis dataset. *Journal of Climate*, **17** (9), 1828–1844.
- Robinson, D. P. and R. X. Black, 2006: Baroclinic development in observations and NASA GSFC general circulation models. *Monthly Weather Review*, **134** (4), 1161–1173, 16.
- Robinson, D. P., R. X. Black, and B. A. McDaniel, 2006: A siberian precursor to midwinter intraseasonal variability in the North Pacific storm track. *Geophysical Research Letters*, **33** (15), 4.
- Uppala, S. M., et al., 2005: The ERA-40 re-analysis. *Quarterly Journal of the Royal Meteorological Society*, **131** (612), 2961–3012, part B.
- Wallace, J. M., G. H. Lim, and M. L. Blackmon, 1988: Relationship between cyclone tracks, anticyclone tracks and baroclinic wave-guides. *Journal of the Atmospheric Sciences*, **45** (3), 439–462.
- Yin, J., 2002: The peculiar behavior of baroclinic waves during the midwinter suppression of the Pacific storm track. Ph.D. thesis, University of Washington, 137 pp.
- Zhang, Y. Q. and I. M. Held, 1999: A linear stochastic model of a GCM’s midlatitude storm tracks. *Journal of the Atmospheric Sciences*, **56** (19), 3416–3435.

List of Tables

- 1 Table comparing feature tracking statistics with Eulerian variance at 160°E
between 20-70°N. 29

variable	$\frac{winter}{fall+spring}$
magnitude (Z)	0.86
number (N)	0.80
area (A)	1.14
velocity (c)	1.03
B_{LAGR}	0.61
$\overline{(Z')^2}$	0.75

TABLE 1. Table comparing feature tracking statistics with Eulerian variance at 160°E between 20-70°N.

List of Figures

- 1 Midwinter suppression of the Pacific storm track, shown as the variance in upper-level geopotential height. (a) Pacific domain, $140^{\circ}\text{E} - 180^{\circ}$, and (b) Atlantic domain, $30^{\circ} - 70^{\circ}\text{W}$. The contour interval is $1500 - m^2$ starting at $2000 - m^2$. This is an update of Fig. 2 in Nakamura (1992), for the ERA-40 dataset between 1958-2001. The data are 2-6 day band-passed filtered using a 4th-order Butterworth filter to obtain daily climatologies. Results are smoothed with a 31-day running mean filter and plotted every five days. Large tick marks on the abscissa correspond to the first day of each month. 33
- 2 Sample of the individual disturbances (randomly selected from the month of November) that cross the longitude 160°E , between $20^{\circ} - 70^{\circ}\text{N}$ (thick black line). Black dots denote genesis location, and gray line indicates the path of individual disturbances. The contour is for 1500-m topography, and shading indicates topography higher than 3km. The boxed regions correspond to the areas where statistics are compiled for the Pacific, Atlantic, and mid-latitude Asian storm tracks in Fig. 7. 34

- 3 Seasonal cycle of the features that were identified in the geopotential height field at 300-hPa. (a) mean amplitude (this is the magnitude, in dm, at the center of the disturbance) of disturbances as they cross 160°E (Pacific storm track), (b) mean monthly frequency of disturbances as they cross 160°E (Pacific storm track), (c) mean amplitude (dm) of disturbances as they cross 50°W (Atlantic storm track), and (d) mean monthly frequency of disturbances as they cross 50°W (Atlantic storm track). Daily climatologies have been smoothed with a 31-day running mean smoother. Tick marks correspond to the first day of each month, and shading indicates 95% confidence intervals as calculated from the student's t-test. 35
- 4 Same as Fig. 3, except for Pacific storm track features that originated (a) over land, mean amplitude (dm), (b) over land, mean monthly frequency, (c) over ocean, mean amplitude (dm), and (d) over ocean, mean monthly frequency. 36
- 5 Same as Fig. 3, except for Pacific storm track features that originated (a) North of 40°N, mean amplitude (dm), (b) North of 40°N, mean monthly frequency, (c) South of 40°N, mean amplitude (dm), and (d) South of 40°N, mean monthly frequency. 37
- 6 Same as Fig. 3, except for features upwind (60°E) and downwind (120°E) of the Tibetan plateau (a) upwind, mean amplitude (dm), (b) upwind, mean monthly frequency, (c) downwind, mean amplitude (dm), and (d) downwind, mean monthly frequency. 38

- 7 Comparison between the actual growth rate in Z at 300-hPa and the near-surface adjusted Eady growth rate, in $dmhr^{-1}$, for (a) the Pacific storm track (20-70°N, 120-160°E), (d) the Atlantic storm track (20-70°N, 70-30°W), and (g) the mid-latitude Asian storm track (40-55°N, 90-120°E). Plotted in (b), (e), and (h) are the monthly average near-surface Eady growth rate expressed as percent growth, $\%hr^{-1}$, for the Pacific, Atlantic, and mid-latitude Asian storm tracks, respectively. Plotted in (c), (f), and (i) are the monthly average feature amplitudes in Z at 300-hPa (dm) for the Pacific, Atlantic, and mid-latitude Asian storm tracks, respectively. In (h), the monthly averaged near surface stability (diamond) and shear (dashed-plus) are also indicated. For (a) - (f), the Eady growth rates are calculated for the layer between 925 - 850-hPa, and for (g) - (i) the Eady growth rate is calculated for the layer between 850 - 775-hPa. 39
- 8 Same as Fig. 3, except for relative vorticity at 300-hPa. In (a) and (c), units are $10^{-5} s^{-1}$. 40

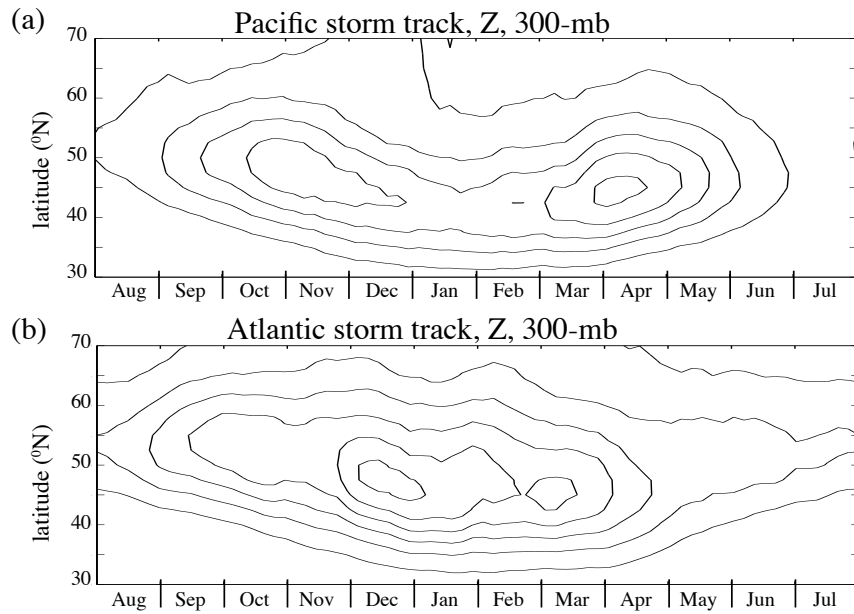


FIG. 1. Midwinter suppression of the Pacific storm track, shown as the variance in upper-level geopotential height. (a) Pacific domain, $140^{\circ}\text{E} - 180^{\circ}$, and (b) Atlantic domain, $30^{\circ} - 70^{\circ}\text{W}$. The contour interval is $1500 - m^2$ starting at $2000 - m^2$. This is an update of Fig. 2 in Nakamura (1992), for the ERA-40 dataset between 1958-2001. The data are 2-6 day band-passed filtered using a 4th-order Butterworth filter to obtain daily climatologies. Results are smoothed with a 31-day running mean filter and plotted every five days. Large tick marks on the abscissa correspond to the first day of each month.

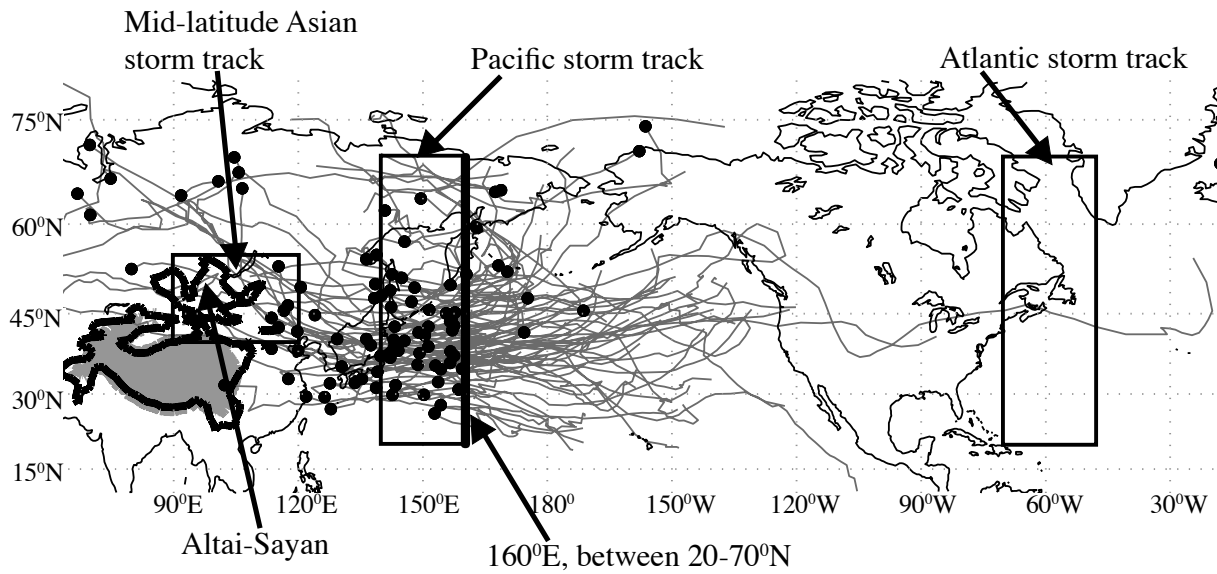


FIG. 2. Sample of the individual disturbances (randomly selected from the month of November) that cross the longitude 160°E, between 20°- 70°N (thick black line). Black dots denote genesis location, and gray line indicates the path of individual disturbances. The contour is for 1500-m topography, and shading indicates topography higher than 3km. The boxed regions correspond to the areas where statistics are compiled for the Pacific, Atlantic, and mid-latitude Asian storm tracks in Fig. 7.

Feature tracking results for Z, 300-hPa

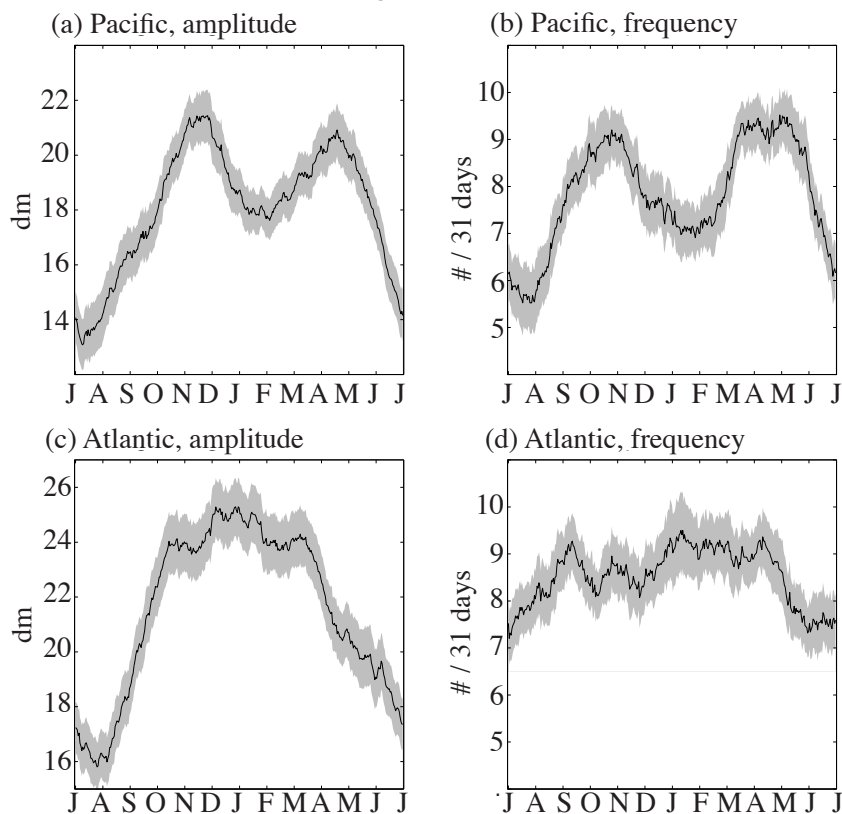


FIG. 3. Seasonal cycle of the features that were identified in the geopotential height field at 300-hPa. (a) mean amplitude (this is the magnitude, in dm, at the center of the disturbance) of disturbances as they cross 160°E (Pacific storm track), (b) mean monthly frequency of disturbances as they cross 160°E (Pacific storm track), (c) mean amplitude (dm) of disturbances as they cross 50°W (Atlantic storm track), and (d) mean monthly frequency of disturbances as they cross 50°W (Atlantic storm track). Daily climatologies have been smoothed with a 31-day running mean smoother. Tick marks correspond to the first day of each month, and shading indicates 95% confidence intervals as calculated from the student's t-test.

Pacific storm track results for Z, 300-hPa

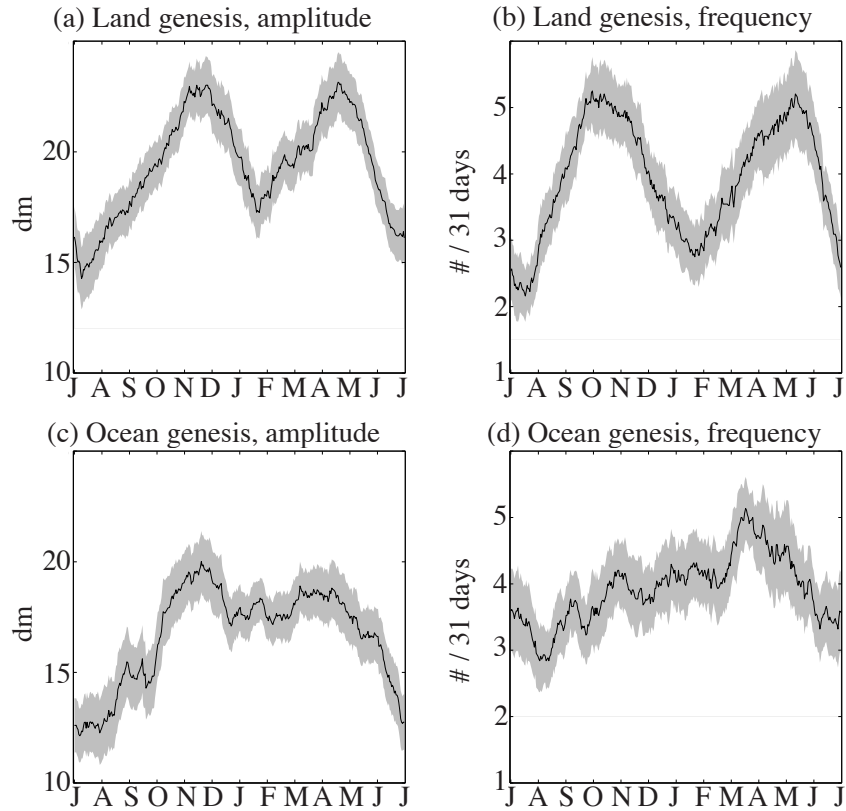


FIG. 4. Same as Fig. 3, except for Pacific storm track features that originated (a) over land, mean amplitude (dm), (b) over land, mean monthly frequency, (c) over ocean, mean amplitude (dm), and (d) over ocean, mean monthly frequency.

Feature tracking results for Z, 300-hPa

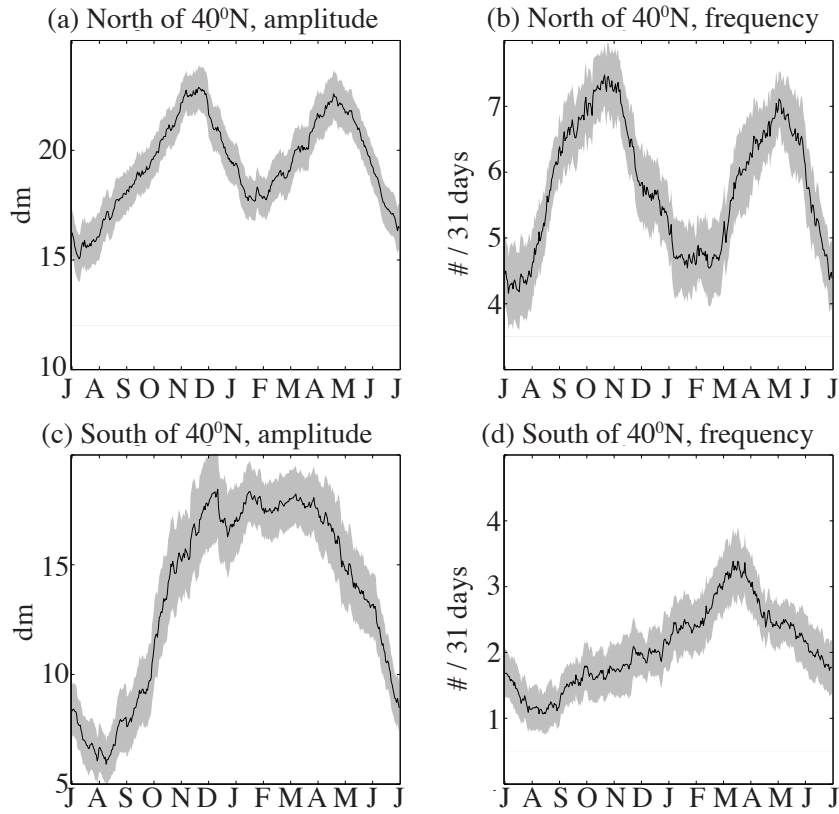


FIG. 5. Same as Fig. 3, except for Pacific storm track features that originated (a) North of 40°N, mean amplitude (dm), (b) North of 40°N, mean monthly frequency, (c) South of 40°N, mean amplitude (dm), and (d) South of 40°N, mean monthly frequency.

Feature tracking results for Z, 300-hPa

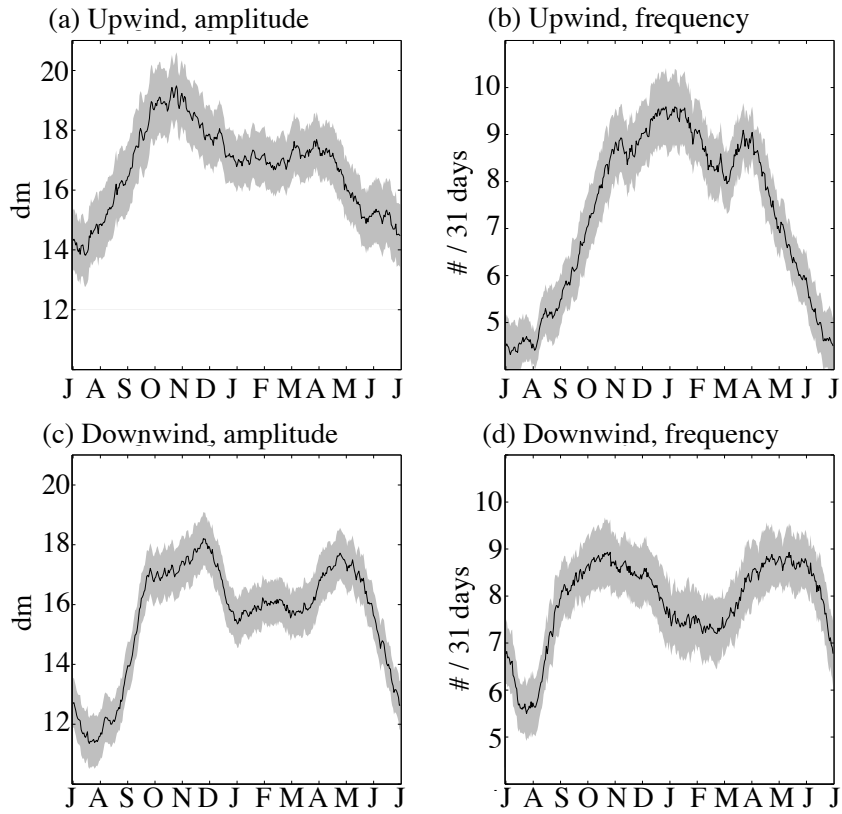


FIG. 6. Same as Fig. 3, except for features upwind (60°E) and downwind (120°E) of the Tibetan plateau (a) upwind, mean amplitude (dm), (b) upwind, mean monthly frequency, (c) downwind, mean amplitude (dm), and (d) downwind, mean monthly frequency.

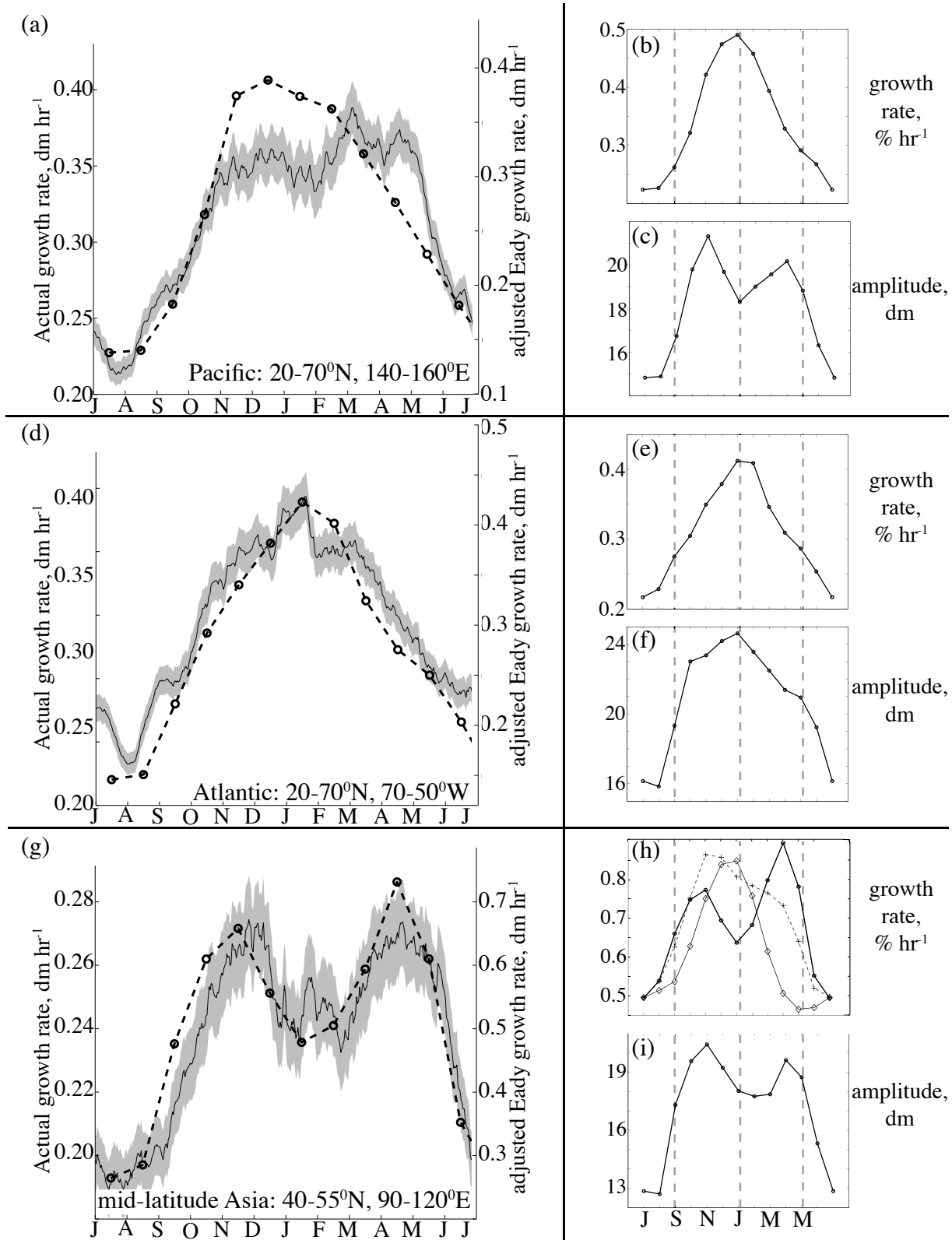


FIG. 7. Comparison between the actual growth rate in Z at 300-hPa and the near-surface adjusted Eady growth rate, in $dm\ hr^{-1}$, for (a) the Pacific storm track (20-70°N, 120-160°E), (d) the Atlantic storm track (20-70°N, 70-30°W), and (g) the mid-latitude Asian storm track (40-55°N, 90-120°E). Plotted in (b), (e), and (h) are the monthly average near-surface Eady growth rate expressed as percent growth, $\% hr^{-1}$, for the Pacific, Atlantic, and mid-latitude Asian storm tracks, respectively. Plotted in (c), (f), and (i) are the monthly average feature amplitudes in Z at 300-hPa (dm) for the Pacific, Atlantic, and mid-latitude Asian storm tracks, respectively. In (b), (e), and (h), the monthly average near-surface growth rate is plotted as a solid line with markers, and the monthly average near-surface growth rate is plotted as a dashed line with markers.

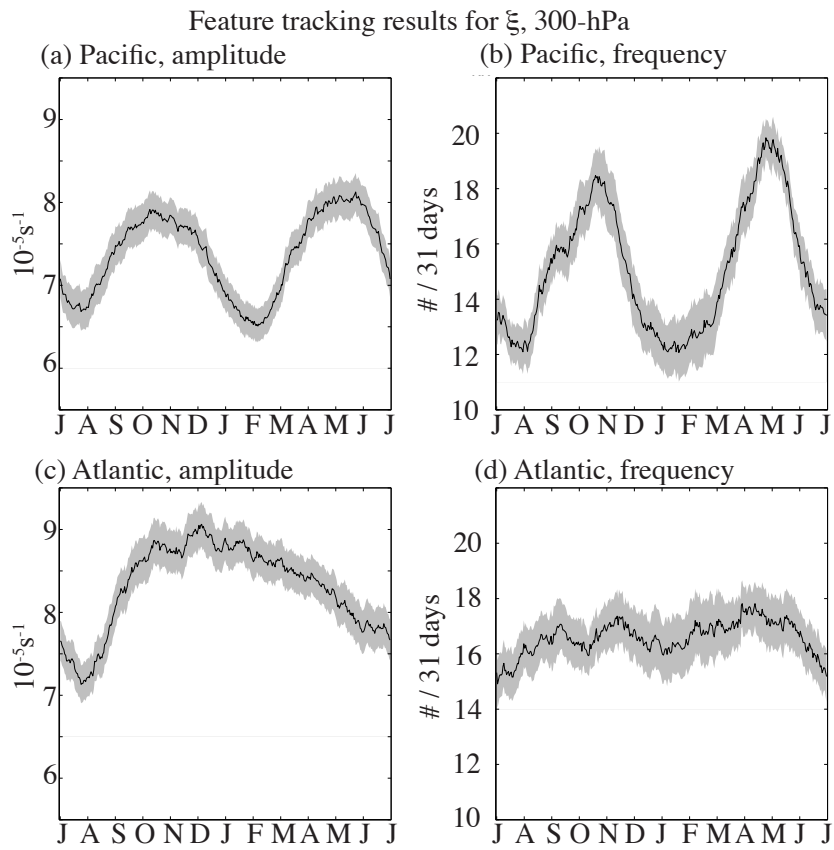


FIG. 8. Same as Fig. 3, except for relative vorticity at 300-hPa. In (a) and (c), units are 10^{-5} s^{-1} .